Sensors & Diagnostics

PAPER

View Article Online
View Journal | View Issue

Check for updates

Cite this: *Sens. Diagn.*, 2024, **3**, 1201

A triphenylamine scaffold for fluorogenic sensing of noxious cyanide *via* the ICT mechanism and its bioimaging application†

Amitav Biswas,[a] Rimi Mukherjee,[b] Atanu Maji,[a] Rahul Naskar,[a] Krishnendu Aich,[a] Nabendu Murmu[b] and Tapan K. Mondal *[a]

A novel triphenylamine benzimidazole based fluorogenic chemosensor named (2*E*,2′*E*)-3,3′-((phenylazanediyl)bis(4,1-phenylene))bis(2-(1*H*-benzo[*d*]imidazol-2-yl)acrylonitrile) (PBIA) has been successfully generated and characterized by varoius spectroscopic techniques. Among various screened anions, only cyanide (CN^-) showed a distinct fluorogenic property towards PBIA. Hence, the optical properties of PBIA were investigated in the presence of cyanide (CN^-) by means of UV-vis spectrophotometry and fluorescence spectroscopy in DMSO, where we observed that, upon treatment with CN^- to the probe solution, the orange fluorescence of the ligand showed a blue shift and the orange fluorescence changed to greenish-yellow under an UV lamp. The hypsochromic shift in fluorescence maxima upon the addition of cyanide was attributed to nucleophilic addition of cyanide to PBIA inhibiting the electron flow within the molecule and disrupting the ICT process. The interaction behind the sensing of cyanide was investigated by ^{1}H-NMR titration, a mass spectroscopic study and DFT calculations, which supported the mechanism. The limit of detection (LOD) was calculated and found to be in the order of 10^{-8} (M). PBIA showed an immediate response in the spectral pattern (<20 s) towards its target cyanide ion, and the effectiveness of the chemosensor was also examined in the presence of competing anions. Furthermore, the practical efficacy of the PBIA was established by a dipstick experiment along with cyanide detection in various natural water resources. Human breast cancer cells MDA-MB 231 were made susceptible to CN^- sensing in a biological system.

Received 17th January 2024,
Accepted 21st May 2024

DOI: 10.1039/d4sd00018h

rsc.li/sensors

Open Access Article. Published on 23 May 2024. Downloaded on 2/10/2026 11:50:29 PM.
This article is licensed under a Creative Commons Attribution 3.0 Unported Licence.

Introduction

We all know that anions play an imperative role in different disciplines, such as biological systems and environmental chemical processes, as well as different technological, clinical and medical processes.[1–4] Among various anions, cyanide is listed as one of the most noxious and lethal chemical substances known to us. Conversely, cyanide has different industrial applications, *i.e.*, in making plastics, papers and herbicides.[5,6] Cyanide is also endlessly used in the synthesis of resins and synthetic fibres, electroplating, refining, leather making, as a chelator in water treatment and metallurgy.[7–10] Again, cyanide salt is majorly used in the extraction of gold from its ore, where the gold elemental substance after complexation with cyanide has reduced oxidation potential; as a result, the substance gets easily oxidized by oxygen to form soluble aurate and dissolves under alkaline conditions, which makes gold easily separable from slag.[11] Despite its enormous applications in various fields, cyanide is still very detrimental to humans even at the minimum dosage of 0.05 mg kg^{-1}.[12] Moreover, WHO has set up an acceptable limit of cyanide of 1.9 μM in drinking water due to its toxic nature.[13] Cyanide can be absorbed in the human body through the skin, lungs and gastrointestinal tract, which leads to acute effects in the human body. Cyanide complex with ferric iron in metalloenzymes leads to histotoxic hypoxia (low oxygen level) by inhibition of cytochrome *c* oxidase, where cyanide gets attached to the active sites of cytochrome oxidase (at cytochrome a3) resulting in the disconnection of mitochondrial oxidative phosphorylation, which further leads to obstruction of cellular respiration.[14–16] Excessive exposure to cyanide leads to poisoning of the respiratory system, paralysis of the central nervous system, haemoglobin poisoning, convulsion, and vomiting with loss of consciousness that eventually lead to death.[17] Therefore, huge

[a] *Department of Chemistry, Jadavpur University, Kolkata-700032, India. E-mail: tapank.mondal@jadavpuruniversity.in*
[b] *Department of Signal Transduction and Biogenic Amines (STBA), Chittaranjan National Cancer Institute, Kolkata-700026, India*

† Electronic supplementary information (ESI) available. See DOI: https://doi.org/10.1039/d4sd00018h

© 2024 The Author(s). Published by the Royal Society of Chemistry

Open Access Article. Published on 23 May 2024. Downloaded on 2/10/2026 11:50:29 PM.
This article is licensed under a Creative Commons Attribution 3.0 Unported Licence.

interest has been sparked in designing and developing new fluorescent chemosensors to detect cyanide and monitor it in environmental samples.

There are several well-established analytical techniques for the qualitative and quantitative detection of cyanide, including atomic absorption spectroscopy (AAS), inductively coupled plasma-mass spectroscopy (ICPMS), inductively coupled plasma emission spectrometry (ICPES), voltammetry, cyanide-selective electrodes, polarography, and chromatography (HPLC).[18–22] However, these techniques have several pitfalls as they require fast sample preparation, trained operators, sophisticated equipment, and portability, and they suffer from cost issues.[23] These methods are also time consuming. Conversely, a fluorescent chemodosimetric approach to detect its guest analytes have gained huge interest due to a simple synthetic procedure, reusability and rapid detection through naked eye.[24]

Generally, the strategy behind the design of cyanide sensors is based upon hydrogen bonding, deprotonation, nanotechnology, supramolecular self-assembly, metal cyanide displacement and nucleophilic addition techniques.[25–31] However, the first few approaches lacked selectivity due to interference by protic solvents and competing ions, whereas the ion displacement technique requires a stabilized metal–ligand complex. On the contrary, a chemosensor based on a nucleophilic addition reaction, known as a chemodosimeter, possesses benefits such as high selectivity and sensitivity, and a rapid response time. Reaction-based chemosensors mainly involve various functional group such as C=C, C=N and C=O, which are selectively attacked by cyanide ion, creating a strong irreversible chemical bond known as a chemodosimeter.[32–34] The photophysical properties of these organic chemodosimeters get disturbed when nucleophilic addition takes place and the electronic properties of these sensors become transformed. Thus, a change in fluorescence signal results due to nucleophilic addition of analytes. Probes detecting cyanide mainly involve various mechanisms, such as hydrogen bonding interaction, intra-molecular charge transfer (ICT), twisted intra-molecular charge transfer (TICT), fluorescence resonance energy transfer (FRET), excited state intra-molecular proton transfer (ESIPT), and photo-induced electron transfer (PET).[35–41] Among these mechanisms, ICT plays a pivotal role in cyanide detection as the push–pull effect between donor and acceptor gets disturbed due to the addition of cyanide, which results in a change in the ICT process within the organic framework.

To date, several donor–π–acceptor (D–π–A) type sensors have been developed to detect trace amount of CN^- ions, based upon intramolecular charge transfer (ICT), where, due to the presence of various subunits such as C=C and C=N, the ICT process is inhibited as a result of the nucleophilic addition that causes the spectral change.[34,42–50] There are also various reported sensors based upon the 1,1-dicyanovinyl group for cyanide sensing.[51–55] A number of chemical motifs have previously been reported, involving indolium, benzyl derivatives, acridinium salts, aldehyde and trifluoroacetyl groups, where cyanide caused a change in conjugation and spectroscopic properties.[56–62]

Hence, taking into account the novel reactivity of cyanide ion, we have successfully synthesized a highly fluorescent chemodosimeter (PBIA) that has a backbone of acceptor–π–donor–π–acceptor (A–π–D–π–A) units. The benzimidazole-2-acetonitrile group present on both sides act as an acceptor group, whereas triphenylamine moiety plays the role of electron donating subunit. The chemodosimeter serves as a fluorescent sensor for the detection of cyanide with high selectivity and sensitivity in DMSO. As cyanide acts as a good nucleophile, it attacks the electrophilic centre of the probe, resulting into a distinguishable change in colour under UV light from orange to greenish-yellow. We have also successfully applied the chemodosimeter for the detection of cyanide in real water samples. A TLC plate experiment was also executed as a qualitative experiment. A biocompatibility study was visualized in MDA-MB-231 cell lines.

Results and discussion

Synthesis of the sensor (PBIA)

Very economically cheap precursors, *i.e.*, triphenyl amine, *o*-phenylene diamine, and ethyl cyanoacetate were used for the synthesis of PBIA. The synthetic design for PBIA is shown in Scheme 1, where compounds '**1**' and '**2**' were prepared using a previously reported procedure.[63,64] Then, 4,4′-(phenylazanediyl)dibenzaldehyde was reacted with 2-(1*H*-benzo[*d*]imidazol-2-yl)acetonitrile in absolute ethanol solvent under reflux conditions in the presence of piperidine, which yielded our desired probe PBIA. Additionally, the PBIA sensor was thoroughly characterized by elemental analysis, ^{1}H NMR, ^{13}C NMR, IR and HRMS spectroscopic methods; the data are given in ESI† (Fig. S1–S6).

Photophysical properties of PBIA

UV-vis spectral studies. We observed the photophysical study of probe PBIA in 100% DMSO medium. In UV-vis absorption study, we noted that the probe PBIA itself shows a low energy absorption band at 455 nm along with a shoulder

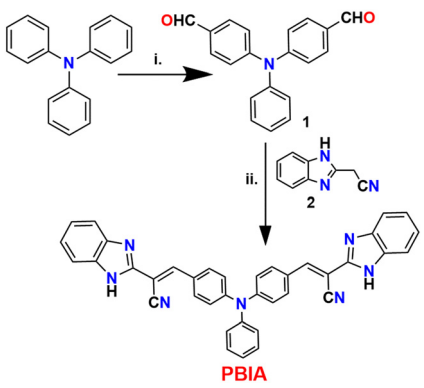

Scheme 1 Synthetic route to the probe (PBIA) (i) DMF, $POCl_3$, 0 °C, 2 h; (ii) EtOH, piperidine, reflux, 3 h.

© 2024 The Author(s). Published by the Royal Society of Chemistry

Open Access Article. Published on 23 May 2024. Downloaded on 2/10/2026 11:50:29 PM.
This article is licensed under a Creative Commons Attribution 3.0 Unported Licence.

peak at 400 nm and a high energy small peak at 340 nm. These energy bands correspond to the ICT character of PBIA, which is generated from its structural observation. PBIA contains a triphenyl-amine group, which is a strong electron donor in nature and phenylacrylonitrile benzimidazole conjugated skeleton moiety, which is an electron acceptor in nature; hence, this charge-separated structure represents a typical A–π–D–π–A framework.

With the gradual addition of CN^-, we observed that the absorption peak at 455 nm tends to decreases with a blue shift. Thus, a new absorption peak appears at 425 nm. Simultaneously, we noted that the shoulder peak at 400 nm and high-energy band at 340 nm disappear, with the generation of two very small peaks at 294 nm and 310 nm, respectively; whereas two distinct isosbestic points were observed at 320 nm and 282 nm (Fig. 1). These shifting of bands to high energy clearly indicates the nucleophilic addition of cyanide to the electron-deficient part of PBIA, which results in distortion in the ICT process and disrupts the electron conjugation between benzimidazole and triphenylamine counterparts. We performed time-dependent absorption spectra where we observed that the curve reaches a minimum within 24 seconds; then, a plateau was observed, indicating completion of the reaction (Fig. S8, ESI†).

Furthermore, to establish the selectivity of our PBIA probe we performed UV-vis studies in the presence of other relevant anions: F^-, Cl^-, Br^-, I^-, HSO_4^-, NO_3^-, SCN^-, ClO_4^-, HSO_3^-, OAc^-, HCO_3^-, CO_3^{2-}, N_3^-, S^{2-}, $S_2O_3^{2-}$, SO_3^{2-} and SO_4^{2-} in DMSO at room temperature; but the addition of these other anions did not show any significant changes to ligand absorption spectra (Fig. S10, ESI†).

Fluorescence spectral study. The probe PBIA itself shows bright orange coloured fluorescence, which occurs due to the strong ICT process within the probe. When excited at 430 nm, it shows a strong emission band with an emission maximum at 570 nm, and the fluorescence quantum yield was calculated to be 0.148. Then, the fluorescence spectra of PBIA were recorded in DMSO with the gradual addition of CN^- (40 μM). We observed that the fluorescence maxima began to decrease with a blue shift, and finally, we observed a new band at 535 nm with an isoemissive point at 520 nm

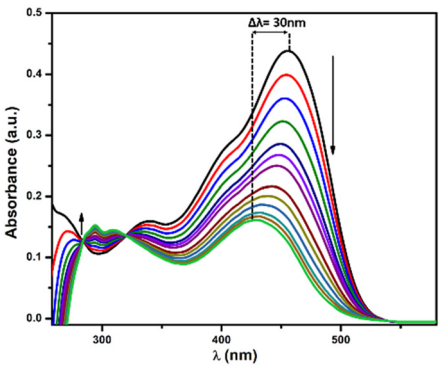

Fig. 1 Change in UV-vis spectrum of PBIA (20 μM) upon the gradual addition of CN^- (40 μM) in DMSO.

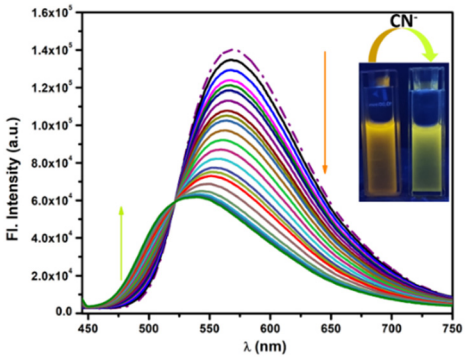

Fig. 2 Change in emission spectra of PBIA (20 μM) upon the gradual addition of CN^- (40 μM) in DMSO. Inset: the change in colour under UV light (λ_{ex} = 430 nm).

(Fig. 2). Hence, we observed a clear blue shift of 35 nm, which clearly accounted for the disruption of the ICT process with a decrease in fluorescence intensity. Subsequently, we also observed a change in the fluorescence colour from orange to greenish-yellow under UV light.

The blue shift of the emission band with a simultaneous decrease in the emission intensity is attributed to the distortion in the ICT process, due to the nucleophilic addition of cyanide to PBIA, forming a PBIA–CN adduct. The quantum yield value also changes to 0.074. We also calculated the quenching constant between PBIA and CN^- using a Stern–Volmer plot, and it was found to be 1.16×10^3 M^{-1} (Fig. S14, ESI†). To further confirm the sensing experiment, we checked the effect of water on the fluorescence intensity of PBIA. From fluorescence spectral studies it was observed that the probe showed maximum fluorescence intensity in DMSO medium: with an increase in the fraction of water, the fluorescence intensity of PBIA decreases with a simultaneous red shift (Fig. S15, ESI†). Hence, we optimized the solvent system to be DMSO alone and conducted all spectroscopic studies in this.

In Commission International de L'Eclairage (CIE) chromaticity coordinates (Fig. 3) we also observed noticeable changes from orange to greenish-yellow with a change in

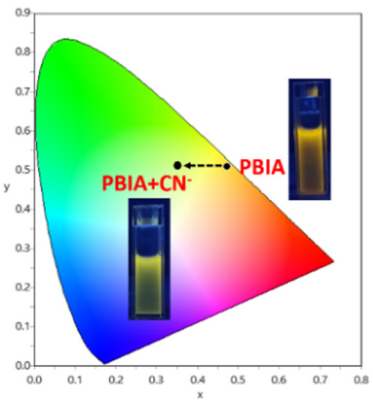

Fig. 3 CIE1931 chromaticity diagram of PBIA probe with cyanide.

Open Access Article. Published on 23 May 2024. Downloaded on 2/10/2026 11:50:29 PM.
This article is licensed under a Creative Commons Attribution 3.0 Unported Licence.

coordinates from (x = 0.4736, y = 0.5073) to (x = 0.3689, y = 0.5160). The fluorescence response was also studied in the presence of other similar relevant anions: F^-, Cl^-, Br^-, I^-, HSO_4^-, NO_3^-, SCN^-, ClO_4^-, HSO_3^-, OAc^-, HCO_3^-, CO_3^{2-}, N_3^-, S^{2-}, $S_2O_3^{2-}$, SO_3^{2-} and SO_4^{2-} in DMSO to reveal whether or not they showed any significant sensing property towards PBIA. We noted that other than a slight decrease in the emission intensity of PBIA, these competitive anions do not show any distinguishable change to the fluorescence pattern of PBIA (Fig. S11, ESI†). Further, for the quantitative measurement of CN^-, we plotted the change in the emission intensity at 570 nm with concentration, and we observed an almost linear plot. The limit of detection (LOD) of PBIA towards cyanide ions was calculated and found to be (6.56 ± 0.26) × 10^{-8} (M), which was established from fluorescence titration data upon the addition of CN to PBIA using the equation, LOD = $K \times (Sb_1/S)$. We used k = 3; Sb_1 is the standard deviation and S stands for the slope of the linear response curve (Fig. S9, ESI†).

Again, since an efficient sensor must detect its guest anion within short span of time, a kinetics study was performed to assess the reaction time of the probe towards CN^-. The fluorescence response timescale was taken in the range of 0–60 seconds. The experiment revealed that the fluorescence intensity of the probe at 570 nm remains almost constant, whereas, in the case of PBIA–CN, the intensity at 570 nm decreases, as the fluorescence maximum decreases with a blue shift as the reaction progresses. The minimum of the curve was reached within 20 s, and we observed a plateau indicating completion of the reaction (Fig. 4). This short span of detection time made it clear that our probe is a potential candidate for the rapid detection of CN^-.

Competitive study. An efficient chemosensor must show selectivity and sensitivity towards its guest analyte. Hence, a competitive experiment was performed to study the efficiency of PBIA in the presence of different biologically and environmentally relevant guest anions. CN^- was added to a solution of PBIA containing other anions such as F^-, Cl^-, Br^-, I^-, HSO_4^-, NO_3^-, SCN^-, ClO_4^-, HSO_3^-, OAc^-, HCO_3^-, CO_3^{2-}, N_3^-, S^{2-}, $S_2O_3^{2-}$, SO_3^{2-} and SO_4^{2-}. Upon excitation at 430 nm, PBIA selectively detected CN^- with an emission intensity

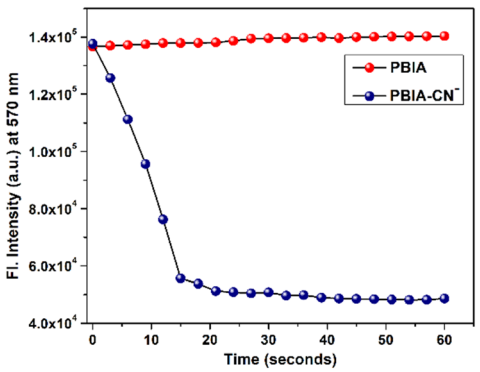

Fig. 4 Time-dependent fluorescence spectrum of PBIA towards CN^- in DMSO.

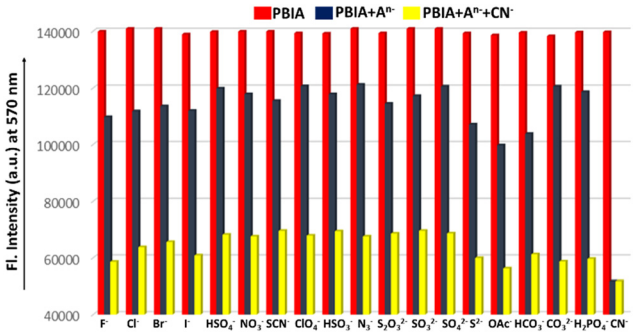

Fig. 5 Competitive experiments of PBIA (20 μM) for CN^- (40 μM) in the presence of common anions (40 μM).

centred around 535 nm in the presence of aforementioned anions. As can be observed from the bar graph represented in Fig. 5, other anions do not alter the intensity pattern of PBIA with fluorescence maxima at 570 nm. The only change was observed when CN^- was added: the fluorescence maximum shifted to 535 nm. Thus, we have represented the bar graph at the fluorescence maximum of 570 nm. This competitive study clearly demonstrates the binding ability of PBIA towards CN^- and anti-interference ability of PBIA towards other anions, which results from the strong nucleophilic character of CN^-, forming a strong adduct of PBIA–CN, even if there are other anions present. This proves the high anti-interference ability of our synthesized probe with an effective signalling aptitude towards CN^-.

pH study. CN^- plays an important role in industrial procedures as well as in biological processes. Hence, to investigate the dependence of our PBIA probe on pH, we recorded the emission spectra of PBIA and PBIA–CN in DMSO solution with pH values ranging from 2.0 to 12.0. It was noted that for free probe PBIA with a decrease in pH (pH < 7), the emission intensity decreases at 570 nm. This is presumably due to protonation of the nitrogen atom disrupting the electron transfer process; whereas we observed that the fluorescence intensity at 570 nm decreases, with a blue shift also in basic conditions, which might result from deprotonation of imidazole protons. For PBIA–CN under strong acidic condition (pH < 5), the fluorescence intensity is also quenched at 535 nm, simultaneously decreasing the intensity at a value of 570 nm. The fluorescence intensity at 535 nm does not alter very much for higher pH values as it shows a blue shift. Hence, the intensity also remains low at 570 nm (Fig. S12, ESI†). It is clear from the plot that the intensity is prominent and shows maximum values only near pH 7. This noteworthy emission maximum near pH 7 indicates that, PBIA is most effective in sensing CN^- in a near-neutral pH (7.2) medium. The effect of pH was also examined in the case of the absorption spectra for PBIA and PBIA–CN in DMSO (Fig. S13, ESI†).

TRPL study. To gain a better insight into the excited-state behaviour, a nanosecond time-resolved fluorescence study (TRPL) is a convenient tool. Hence, we took the probe (PBIA) and adduct (PBIA–CN) in DMSO and performed the study.

© 2024 The Author(s). Published by the Royal Society of Chemistry

Open Access Article. Published on 23 May 2024. Downloaded on 2/10/2026 11:50:29 PM.
This article is licensed under a Creative Commons Attribution 3.0 Unported Licence.

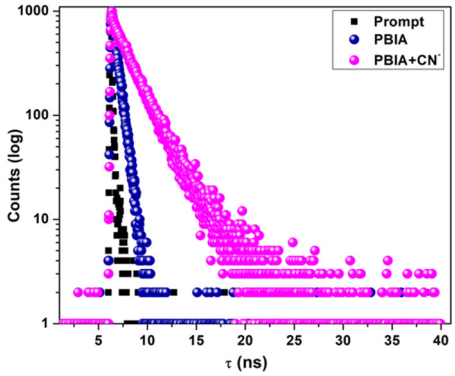

Fig. 6 Time-resolved fluorescence decay of PBIA (●●●), PBIA–CN adduct (●●●) and prompt (■■■) in DMSO (λ_{ex} = 430 nm).

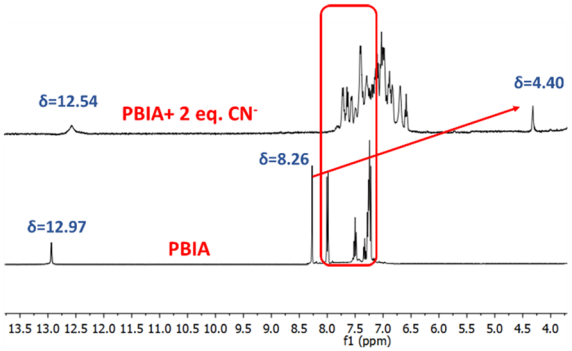

Fig. 7 ^{1}H-NMR spectra of PBIA and PBIA + CN^- (2 equivalent) in DMSO-d_6.

The fluorescence lifetime decay plots were fitted using a mono-exponential function of PBIA and bi-exponential function of the PBIA–CN adduct with acceptable χ^2 values (Fig. 6). For PBIA, it was calculated that τ = 0.50 ns (χ^2 = 1.07) and for the PBIA–CN adduct, the value increased to τ = 1.92 ns (χ^2 = 1.01). The increase in lifetime also supports the sensing mechanism, where in the case of PBIA, due to a stronger ICT the energy gap is low, resulting in a lower lifetime. Conversely, for the PBIA–CN adduct, the energy gap is high owing to a weak ICT triggering a longer lifetime. Equations $\tau^{-1} = K_r + K_{nr}$ and $K_r = \varphi_f/\tau$ were also implemented to calculate the values of the radiative rate constant K_r and total non-radiative rate constant K_{nr} (Table S2, ESI†). The changes in the values of τ, K_r and K_{nr} reflect the formation of the CN^- adduct, which shows a longer lifetime compared to the free probe PBIA itself. Hence, the fluorescence lifetime measurement experiment shows that PBIA can be used as a lifetime-based sensor for cyanide ion.

Possible sensing mechanism

A possible sensing mechanism of the PBIA probe towards CN^- was investigated by ^{1}H-NMR spectroscopy. In the ^{1}H-NMR spectrum of free PBIA, we noted that the –NH proton resonates at 12.97 ppm, and the resonance signal of aromatic protons appears to be in the range between 8.00 and 7.21 ppm, while the vinylic proton corresponds to a peak at 8.26 ppm (Fig. S1, S5, and S6 ESI†). In the case of the PBIA–CN adduct, we observed that the –NH peak remains as it is with a slight upfield shift to 12.54 ppm. Additionally, in the case of the aromatic protons it was noted that they were also shifted to the upfield region ranging from 7.76 to 6.18 ppm, which was due to the development of a negative charge in the PBIA–CN adduct (Fig. S16, ESI†). Moreover, broadening of the aromatic region was observed, which could be attributed to the interaction occurring *via* pi-stacking between the aromatic rings of PBIA and large cationic tetrabutylammonium group.[65] This clearly indicates that conjugation between the triphenyl amine group and benzimidazole unit breaks down, whereas the vinylic proton, which was resonating at 8.26 ppm, disappeared in the PBIA–CN adduct. The new signal appeared in the upfield region at 4.40 ppm, indicating the formation of the PBIA–CN adduct (Fig. 7). The formation of PBIA–CN species is also supported by HRMS spectroscopy. In the mass spectrum, the peak at 634.25 (m/z) confirms the formation of a (PBIA + $2CN^-$) adduct (Fig. S10†). The Jobs plot by the absorbance method also supported the binding ratio of 1 : 2 between PBIA and CN^- (Fig. S7, ESI†). Thus, these results disclose the nucleophilic addition of cyanide at the cyano vinyl position (the β position of the C=C bond), which leads to the conversation of sp^2-hybridized carbon to sp^3 hybridization (Fig. 8). We also compared it with some recently reported chemosensors detecting CN^-, in terms of their solvent system, LOD values and detection type in Table S3, ESI.†

Dipstick experiment: detection of CN^- using a TLC plate

To detect toxic analytes successfully, a portable solid platform sensing tool is convenient. Hence, we used the rational analytical technique known as a dipstick experiment to increase the potential application of our probe. To carry out this experiment, thin-layer chromatography (TLC) plates were first submerged in a solution of PBIA in DMSO (2×10^{-4} M),

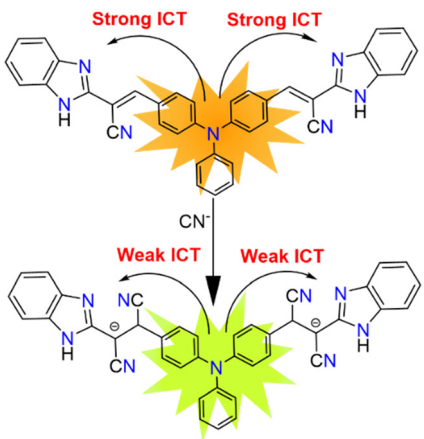

Fig. 8 Probable sensing mechanism of PBIA with CN^-.

Open Access Article. Published on 23 May 2024. Downloaded on 2/10/2026 11:50:29 PM.
This article is licensed under a Creative Commons Attribution 3.0 Unported Licence.

and then, they were kept aside for a few minutes so that the solvent gets evaporated. Subsequently, the TLC plates were immersed in an aqueous solution (2×10^{-3} M) of cyanide and kept open for the solvent to evaporate so that the plates dried out. Under a hand-held UV light, we observed that the TLC plate coated with PBIA showed a brownish colour, whereas when it was immersed in CN^- solution its colour changed to greenish-yellow (Fig. 9). Thus, PBIA shows a difference in colour in the coated TLC platform upon interaction with CN^-, which we can distinguish instinctively. Hence, we can conclude that, without any sophisticated instrumental analysis by simply using a transportable solid-state platform, prompt qualitative naked-eye detection of cyanide is possible.

Real sample analysis

Nowadays, water bodies have become polluted as cyanide from different industrial and commercial sources is dumped into water-bodies endangering aquatic life. Thus, the development of an analytical method for the quantitative detection of CN^- in wastewater is of great importance. To corroborate the practicality of our approach, the detection of CN^- was performed in real samples. Drinking water, university campus lake water and tap water (from the laboratory) were collected and analysed according to a previously reported procedure.[66–70] Collected water samples were filtered using Whatman no. 1 filter paper to remove suspended particles. Then, the standard addition technique was used to calculate the CN^- concentration in water samples, which involved the addition of different increasing concentrations (10, 20, and 30 μM) of CN^- to the above-mentioned water samples (Fig. S21–S23 ESI†). Standard curves were obtained by dissolving CN^- in deionized water. Then, from the experimental data of Table 1, the recovery % was calculated, which shows that it lies within the range from 96.1% to 99.06%. Hence, this experimental data demonstrates the reliability of the PBIA sensor to detect CN^- in different varieties of environmental water samples.

Cell study

Cytotoxicity assay. The cytotoxicity of PBIA was evaluated on the MDA-MB231 human breast cancer cell line using the MTT method. Cells were seeded on a 96-well plate and kept in an incubator for 24 h for attachment of the cells. The cells were treated with the probe PBIA ranging from 20 μM to 640 μM for 24 h (Fig. S20†). The IC_{50} of the chemosensor PBIA was found to be 179.727 μM.

Cellular imaging by fluorescence microscopy. MDA-MB-231 cells were incubated with the probe PBIA; in one group and in another group, the cells were incubated with cyanide along with the probe PBIA. However, no morphological changes in the cells were noted with the treatment. An orange fluorescence was observed in the cells treated with the probe PBIA. Hence, we can conclude from Fig. 10 that the PBIA probe can pass the cell membrane. Upon brief exposure of the cells to cyanide, the cells were found to exhibit green fluorescence whose intensity increases with time, as demarcated in Fig. 10. Bright field images are also shown to indicate the morphological changes with the treatment of the probe PBIA along with cyanide.

Table 1 Recovery % experiment for CN^- detection in various natural water samples

Source	CN^- added (μM)	CN^- recovery (μM)	Recovery (%)
Drinking water	10	9.79	97.9
	20	19.69	98.45
	30	29.56	98.53
Tap water	10	9.61	96.1
	20	19.29	96.45
	30	29.23	97.43
Jadavpur University campus lake water	10	9.86	98.6
	20	19.75	98.75
	30	29.72	99.06

Computational study

To obtain a comprehensive view of the reaction mechanism involved between the probe PBIA with CN^-, we performed theoretical calculations. Geometry optimization of PBIA and

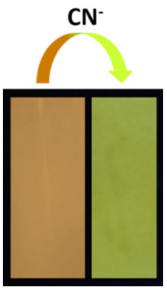

Fig. 9 Pictures of TLC plates after immersion in DMSO solutions of PBIA and PBIA–CN under a hand-held UV chamber. [PBIA] = 2×10^{-4} M, [CN^-] = 2×10^{-3} M. Excitation wavelength of the UV light is 346 nm.

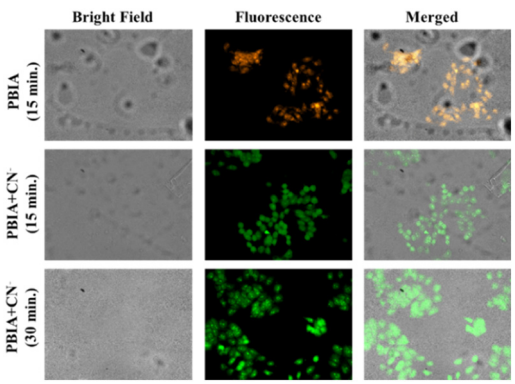

Fig. 10 Fluorescence microscopy images of MDA-MB-231 cells treated with ligand PBIA and PBIA + CN^- after 15 min and 30 min under bright, fluorescence and a merged field (orange channel: 570–610 nm; green channel: 525–555 nm).

© 2024 The Author(s). Published by the Royal Society of Chemistry

Open Access Article. Published on 23 May 2024. Downloaded on 2/10/2026 11:50:29 PM.
This article is licensed under a Creative Commons Attribution 3.0 Unported Licence.

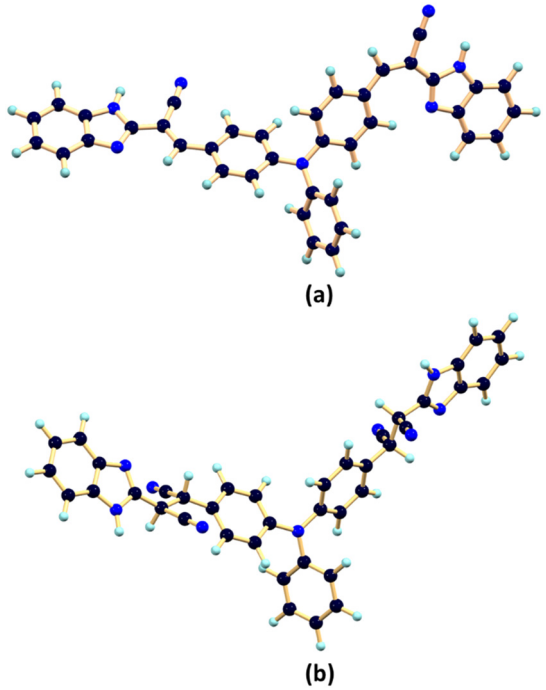

Fig. 11 Optimized structure of (a) PBIA and (b) PBIA–CN calculated by the DFT/B3LYP/6-31+G(d) method.

PBIA–CN were carried out by the DFT/B3LYP/6-31+G(d) method using the Gaussian 09 program. Fig. 11(a) and (b) represents the optimized structures of PBIA and PBIA–CN. Moreover, the contour plots of some selected molecular orbitals of PBIA and PBIA–CN adduct are displayed in Fig. S18 and S19.†

Furthermore, from the HOMO of free PBIA, it is evident that the electron cloud is distributed throughout the entire molecule, which results from the π-conjugation and ICT transition. For the PBIA–CN adduct, we observed that the HOMO electron cloud is distributed mainly on the triphenyl moiety, due to the nucleophilic addition of CN disrupting π-electron conjugation. Due to the noteworthy difference in π-conjugation, the structures of PBIA and PBIA–CN are different. This is evident for different ICT processes responsible for different energy transitions in both cases. Additionally, the energy gap between the HOMO and LUMO for free PBIA was calculated and found to be 3.22 eV, whereas for the PBIA–CN adduct, the HOMO–LUMO energy gap increased considerably to 4.38 eV (Fig. 12). This is expected as the cyanide addition breaks the π-conjugation, increasing the energy gap, weakening the electronic transition and fluorescence property. Moreover, the increase in the HOMO–LUMO energy gap for the PBIA–CN adduct reflected the blue shift in UV-vis spectra. To gain an insight into electronic transitions, time-dependent density functional theory (TDDFT) was performed by the CPCM method on the optimized geometries, and the results are summarized in Table S1.† The calculated transitions agreed well with the blue shift in the UV-vis spectra, which was observed upon the addition of CN^- to PBIA.

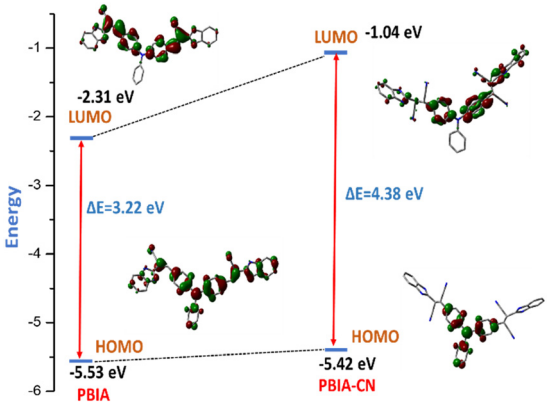

Fig. 12 Calculated frontier molecular orbitals for PBIA and PBIA–CN with their orbital energies using the B3LYP/6-31+G(d) basis set.

Conclusions

To summarize, we have explored the design and synthesis of a novel triphenylamine benzimidazole based sensor PBIA, which showed a selective response towards cyanide ion in DMSO medium. The detection of cyanide in the highly conjugated system of PBIA is based upon the nucleophilic addition of cyanide, which brings out the change in the mode of ICT mechanism with a hypsochromic shift in absorption and fluorescence spectroscopy. Theoretical calculations also support the mechanism. The spectral change depicts excellent selectivity towards cyanide ions along with a rapid interaction time (within 20 s). The limit of detection was found to be of the order of 10^{-8} (M). Moreover, the real-time application of the chemosensor was successfully utilized for the detection of cyanide in real water samples and by TLC plate experiment. Additionally, the live cell imaging experiment demonstrates the capability for sensing intracellular cyanide.

Experimental

Materials and instrumentations

All the reagents and organic chemicals used in the synthesis of PBIA, including *o*-phenylenediamine, ethyl cyanoacetate and triphenylamine, were purchased from Sigma Aldrich and used without further purification, while the other solvents used were available from commercial sources. DMSO and other solvents used for spectroscopic studies were of HPLC grade. For ^{1}H and ^{13}C NMR spectra a Bruker (AC) 400 MHz instrument was used. DMSO-d_6 was used as a solvent using TMS as an internal standard of ~0.05 M concentration. The chemical shifts were reported in δ units of parts per million (ppm). HRMS mass spectra were recorded on a Waters (Xevo G2 Q-TOF) mass spectrometer. For elemental analysis a 2400 Series-II CHN analyzer, Perkin Elmer, USA was used. The infrared spectrum of the probe was recorded using an RX-1 PerkinElmer spectrophotometer by preparing a KBr pellet of the sample. We used a Shimadzu UV-1900i

Open Access Article. Published on 23 May 2024. Downloaded on 2/10/2026 11:50:29 PM. This article is licensed under a Creative Commons Attribution 3.0 Unported Licence.

spectrophotometer to measure the UV-vis spectra. The emission property was measured using a Shimadzu RF-6000 fluorescence spectrophotometer at room temperature (298 K). Luminescence lifetime measurements were carried out using a time-correlated single photon counting setup from Horiba Jobin Yvon. Then, the fluorescence decay data were placed on a Hamamatsu MCP photomultiplier (R3809) and analysed using EZ time software. Merck 60 F254 plates of 0.25 mm thickness were used for thin layer chromatography (TLC) and dipstick experiments. For the column chromatographic technique we used a silica gel of mesh 200–300, where petroleum benzene and ethyl acetate were used as solvents.

UV-vis and fluorescence methods

For the UV-vis study, a stock solution of the PBIA probe (20 μM) was prepared in DMSO. Deionized water was used to make all the solutions of guest anions using their sodium salts (40 μM), and for the solution of cyanide ions, tetrabutylammonium cyanide salt was used. Spectra were recorded using solutions containing PBIA probe and an increasing concentration of guest anions. All the solutions were prepared separately. Similarly, for fluorescence titrations, stock solutions were prepared using similar procedures, and then, the spectra were recorded by means of the fluorescence method. The excitation wavelength used was 435 nm (where the excitation slit was 10.0, and the emission slit was 10.0). The detection limit was calculated using the fluorescence titration data.

pH solution preparation method

For the pH study, we also prepared a stock solution of the probe, PBIA (10 μM) in DMSO (at 25 °C). The pH of the solution was adjusted by using an aqueous solution of 1 M HCl and 1 M NaOH. For titration of probe solutions, different concentrations of acids and bases were prepared separately while adjusting the pH, and the spectra of these solutions were recorded through UV-vis and fluorescence techniques. Similarly, we executed titration of probe (PBIA) in the presence of CN^- while recording the pH.

Synthesis of 4,4′-(phenylazanediyl)dibenzaldehyde (1)

This was prepared using a previously reported procedure.[63]

Synthesis of 2-cyanomethylbenzimidazole (2)

This was previously synthesized by our group.[64]

Synthesis of (2*E*,2′*E*)-3,3′-((phenylazanediyl)bis(4,1-phenylene)) bis(2-(1*H*-benzo[*d*]imidazol-2-yl)acrylonitrile) (PBIA)

First 4,4′-(phenylazanediyl)dibenzaldehyde (0.30 g, 1 mmol) was taken in a round-bottomed flask and dissolved in ethanolic solution. Then, to the ethanolic solution, 2-cyanomethylbenzimidazole (0.31 g, 2 mmol) was added, and the whole mixture was refluxed with a catalytic amount of piperidine under an inert atmosphere. After 3 hours, we observed a deep brown coloured precipitate within the reaction mixture. Then, the reaction mixture was allowed to cool at room temperature. The brown precipitate was collected through filtration, washed with EtOH and dried. Then, column chromatography was performed to further purify the product. The yield was calculated to be, 0.452 g, 78%.

^{1}H NMR (400 MHz, DMSO-d_6). δ (ppm) 12.97 (s, 2H), 8.26 (s, 2H), 7.99 (d, 4H, J = 8.76 Hz), 7.50 (t, 2H, J = 7.8 Hz), 7.32 (t, 1H, J = 7.6 Hz), and 7.28–7.21 (m, 14H).

^{13}C NMR (100 MHz, DMSO-d_6). δ (ppm) 149.5, 148.4, 145.6, 144.8, 131.9, 130.8, 127.6, 127.5, 127.3, 126.6, 123.9, 123.2, 122.2, 117.1, and 99.9.

Anal. Calc. for $C_{38}H_{25}N_7$ (PBIA). Calc. (%) C 78.74, H 4.35, and N 16.91. Found (%), C 78.58, H 4.46, and N 16.96.

IR (cm^{-1}, KBr). υ(C=N) 1581.32, υ(C≡N) 2239.03, υ(C–H) 3048.10, and υ(N–H) 3244.28.

HRMS. Calculated for $C_{38}H_{25}N_7$ $[M + H]^+$, (m/z) = 580.2249; found = 580.1038.

Theoretical study

The Gaussian 09 program package was used for theoretical interpretation.[71] The geometries for PBIA and PBIA–CN were optimized using density functional theory (DFT) at the B3LYP level for the compounds,[72,73] where 6-31+G(d) was assigned as the basis set.[74] Vibrational frequency calculations were performed to ensure that the optimized geometries stand for the local minima with only positive eigen values. Vertical electronic excitations, which were based on B3LYP-optimized geometries, were computed using the time-dependent density functional theory (TDDFT) formalism in DMSO using the conductor-like polarizable continuum model (CPCM).[75–80]

Cell culture and treatment

A human breast cancer cell line (MDA-MB-231) was obtained from the National Centre for Cell Science, Pune, India and maintained in DMEM high glucose (Gibco, Life Technologies) supplemented with 10% fetal bovine serum (FBS) (Gibco, Life Technologies, USA) and 1% penicillin streptomycin. All cell lines were stored at 37 °C in a humidified CO_2 incubator. The cells were given at least two passages before commencing the experiments.

Live cell imaging study

The MDA-MB-231 cells were seeded and left to adhere overnight on a six-well plate containing acid-washed 22 × 22 mm glass cover slips positioned at the bottom of each well. In addition to the control, 10 μM of the PBIA chemosensor along with 15 μM of cyanide were added to each well containing cells. The cells were then fixed with methanol and rinsed with 0.5% phosphate buffer saline Tween (PBST) twice, followed by 1× PBS three times. The cover slips were then put on a glass slide with glycerol and viewed at 40× magnification using a fluorescence microscope (Olympus).

© 2024 The Author(s). Published by the Royal Society of Chemistry

Open Access Article. Published on 23 May 2024. Downloaded on 2/10/2026 11:50:29 PM. This article is licensed under a Creative Commons Attribution 3.0 Unported Licence.

Conflicts of interest

There are no conflicts to declare.

Acknowledgements

The authors thank CSIR (No. 01(2992)/19/EMR-II) and SERB (No. EEQ/2018/000266), New Delhi, India for the financial support. A. Biswas thanks CSIR (File No. 09/096(1023)/2020-EMR-I) New Delhi, India for providing the fellowship.

Notes and references

1 R. Sakai, T. Satoh and T. Kakuchi, Polyacetylenes as colorimetric and fluorescent chemosensor for anions, *Polym. Rev.*, 2017, **57**, 159–174.
2 Y. Liu, Y. Hu, S. Lee, D. Lee and J. Yoon, Fluorescent and colorimetric chemosensors for anions, metal ions, reactive oxygen species, biothiols, and gases, *Bull. Korean Chem. Soc.*, 2016, **37**, 1661–1678.
3 P. Molina, F. Zapata and A. Caballero, Anion recognition strategies based on combined noncovalent interactions, *Chem. Rev.*, 2017, **117**, 9907–9972.
4 S. H. Park, N. Kwon, J. H. Lee, J. Yoon and I. Shin, Synthetic ratiometric fluorescent probes for detection of ions, *Chem. Soc. Rev.*, 2020, **49**, 143–179.
5 A. Alvillo-Rivera, S. Garrido-Hoyos, G. Buitron, P. ThangarasuSarasvathI and G. Rosano-Ortega, Biological treatment for the degradation of cyanide: A review, *J. Mater. Res. Technol.*, 2021, **12**, 1418–1433.
6 K. Grossmann, Auxin herbicides: current status of mechanism and mode of action, *Pest Manage. Sci.*, 2010, **66**, 113–120.
7 G. C. Miller and C. A. Pritsos, Cyanide Social, Industrial and Economic Aspects, in *Proceedings of the TMS Annual Meeting*, 2001, p. 73.
8 D. W. Boening and C. M. Chew, A critical review: general toxicity and environmental fate of three aqueous cyanide ions and associated ligands, *Water, Air, Soil Pollut.*, 1999, **109**, 67–79.
9 Z. C. Xu, X. Q. Chen, H. N. Kim and J. Yoon, Sensors for the optical detection of cyanide ion, *Chem. Soc. Rev.*, 2010, **39**, 127–137.
10 J. Ma and P. K. Dasgupta, Recent developments in cyanide detection: a review, *Anal. Chim. Acta*, 2010, **673**, 117–125.
11 T. Z. Sadyrbaeva, Gold(III) recovery from non-toxic electrolytes using hybrid electrodialysis–electrolysis process. Separation and purification technology, *Sep. Purif. Technol.*, 2012, **86**, 262–265.
12 C. Harper and S. Goldhaber, *Toxicological Profile for Cyanide*, Department of Health and Human Services Agency for Toxic Substances and Disease Registry, Atlanta, 1997.
13 T. Zhu, Z. Li, C. Fu, L. Chen, X. Chen, C. Gao, S. Zhang and C. Liu, Development of an anthraquinone-based cyanide colorimetric sensor with activated C–H group: large absorption redshift and application in food and water samples, *Tetrahedron*, 2020, **76**, 131479.
14 L. Nelson, Acute cyanide toxicity: mechanisms and manifestations, *J. Emerg. Nurs.*, 2006, **32**, S8–S11.
15 J. Y. Noh, I. H. Hwang, H. Kim, E. J. Song, K. B. Kim and C. Kim, Salicylimine-based colorimetric and fluorescent chemosensor for selective detection of cyanide in aqueous buffer, *Bull. Korean Chem. Soc.*, 2013, **34**, 1985.
16 B. Vennesland, E. E. Comm, C. J. Knownles, J. Westly and F. Wissing, *Cyanide in Biology*, Academic Press, London, 1981.
17 C. Baird and M. Cann, *Environmental Chemistry*, Freeman, New York, 2005.
18 S. Mardanya, S. Karmakar, M. Bar and S. Baitalik, Pyrene-biimidazole based Ru(II) and Os(II) complexes as highly efficient probes for the visible and near-infrared detection of cyanide in aqueous media, *Dalton Trans.*, 2015, **44**, 21053.
19 Z. Q. Hu, X. M. Wang, Y. C. Feng, L. Ding, M. Li and C. S. Lin, A novel colorimetric and fluorescent chemosensor for acetate ions in aqueous media based on a rhodamine 6G–phenylurea conjugate in the presence of Fe(III) ions, *Chem. Commun.*, 2011, **47**, 1622.
20 A. Balamurugan and H. Lee, Aldoxime-derived water-soluble polymer for the multiple analyte sensing: consecutive and selective detection of Hg^{2+}, Ag^{+}, ClO^{-}, and cysteine in aqueous media, *Macromolecules*, 2015, **48**, 3934.
21 J. B. Chae, H. J. Jang and C. Kim, Sequential detection of $Fe^{3+/2+}$ and pyrophosphate by a colorimetric chemosensor in a near-perfect aqueous solution, *Photochem. Photobiol. Sci.*, 2017, **16**, 1812.
22 H. J. Jang, H. M. Ahn, M. S. Kim and C. Kim, A highly selective colorimetric chemosensor for sequential detection of Fe^{3+} and pyrophosphate in aqueous solution, *Tetrahedron*, 2017, **73**, 6624.
23 I. G. Casella and M. Gatta, Electrocatalysis and Detection of Carbohydrates by Anion-Exchange Chromatography at a Gold Substrate Electrode Modified with Nickel Cyanide Ions, Electroanalysis: An International Journal Devoted to Fundamental and Practical Aspects of Electroanalysis, *Electroanalysis*, 2001, **13**, 549–554.
24 A. Kumar, E. Jeong, N. Youngwoo and P. S. Chae, Fluorescent-based ratiometric sensors as emerging tools for CN^{-} detection: Chemical structures, sensing mechanisms and applications, *Methods*, 2024, **222**, 57–80.
25 C. Yin, F. Huo, M. Xu, C. L. Barnes and T. E. Glass, Special recognition on HS^{-}/CN^{-} colorimetric and fluorescent imaging material for endogenous H_2S based on nucleophilic addition, *Sens. Actuators, B*, 2017, **252**, 592–599.
26 W. J. Qu, H. H. Yang, J. P. Hu, P. Qin, X. X. Zhao, Q. Lin, H. Yao, Y. M. Zhang and T. B. Wei, A novel bis-acylhydrazone supramolecular gel and its application in ultrasensitive detection of CN^{-}, *Dyes Pigm.*, 2021, **186**, 108949.
27 T. B. Wei, J. D. Ding, J. F. Chen, B. B. Han, X. M. Jiang, H. Yao, Y. M. Zhang and Q. Lin, A cyanide-triggered hydrogen-bond-breaking deprotonation mechanism: fluorescent detection of cyanide using a thioacetohydrazone-functionalized bispillar [5] arene, *New J. Chem.*, 2018, **42**, 1271–1275.
28 P. R. Lakshmi, P. S. Kumar and K. P. Elango, A simple fluorophore-imine ensemble for colorimetric and fluorescent detection of CN^{-} and HS^{-} in aqueous solution, *Spectrochim. Acta, Part A*, 2020, **229**, 117974.

© 2024 The Author(s). Published by the Royal Society of Chemistry

Open Access Article. Published on 23 May 2024. Downloaded on 2/10/2026 11:50:29 PM. This article is licensed under a Creative Commons Attribution 3.0 Unported Licence.

29 B. Aydıner, Ö. Şahin, D. Çakmaz, G. Kaplan, K. Kaya, Ü. Ö. Özdemir, N. Seferoğlu and Z. Seferoğlu, A highly sensitive and selective fluorescent turn-on chemosensor bearing a 7-diethylaminocoumarin moiety for the detection of cyanide in organic and aqueous solutions, *New J. Chem.*, 2020, **44**, 19155–19165.

30 N. Assadollahnejad, M. Kargar, H. R. Darabi, N. Abouali, S. Jamshidi, A. Sharifi, K. Aghapoor and H. Sayahi, A new ratiometric, colorimetric and "turn-on" fluorescent chemosensor for the detection of cyanide ions based on a phenol–bisthiazolopyridine hybrid, *New J. Chem.*, 2019, **43**, 13001–13009.

31 S. Paul, K. Debsharma, S. Dey, S. Halder, K. Jana and C. Sinha, Naphthyl-azine–aggregation induced emission, reversible acidochromism, cyanide sensing and its application in intracellular imaging, *Mater. Adv.*, 2023, **4**, 3874–3891.

32 J. L. Sessler and D. G. Cho, The benzil rearrangement reaction: trapping of a hitherto minor product and its application to the development of a selective cyanide anion indicator, *Org. Lett.*, 2008, **10**, 73–75.

33 Y. Kim, H. Zhao and F. P. Gabbaï, Sulfonium boranes for the selective capture of cyanide ions in water, *Angew. Chem., Int. Ed.*, 2009, **48**, 4957–4960.

34 A. Maji, A. Biswas, A. Das, S. Gharami, K. Aich and T. K. Mondal, A novel carbazole-benzothiazole-based chemodosimeter for the chromogenic and fluorogenic recognition of CN^-, *New J. Chem.*, 2023, **47**, 11557–11564.

35 K. Xiong, F. Huo, C. Yin, Y. Yang, J. Chao, Y. Zhang and M. Xu, A off-on green fluorescent chemosensor for cyanide based on a hybrid coumarin hemicyanine dye and its bioimaging, *Sens. Actuators, B*, 2015, **220**, 822–828.

36 S. Goswami, S. Paul and A. Manna, FRET based selective and ratiometric 'nakedeye' detection of CN^- in aqueous solution on fluorescein–Zn–naphthalene ensemble platform, *Tetrahedron Lett.*, 2014, **55**, 3946–3949.

37 S. H. Park, N. Kwon, J. H. Lee, J. Yoon and I. Shin, Synthetic ratiometric fluorescent probes for detection of ions, *Chem. Soc. Rev.*, 2020, **49**, 143–179.

38 X. Lv, J. Liu, Y. Liu, Y. Zhao, M. Chen, P. Wang and W. Guo, A ratiometric fluorescent probe for cyanide based on FRET, *Org. Biomol. Chem.*, 2011, **9**, 4954–4958.

39 N. Gimeno, X. Li, J. R. Durrant and R. Vilar, *Chem. – Eur. J.*, 2008, **14**, 3006–3018.

40 A. C. Sedgwick, L. Wu, H. H. Han, S. D. Bull, X. P. He, T. D. James, J. L. Sessler, B. Z. Tang, H. Tian and J. Yoon, Excited-state intramolecular proton-transfer (ESIPT) based fluorescence sensors and imaging agents, *Chem. Soc. Rev.*, 2018, **47**, 8842–8880.

41 W. J. Qu, W. T. Li, H. L. Zhang, T. B. Wei, Q. Lin, H. Yao and Y. M. Zhang, A rational designed fluorescent and colorimetric dual-channel sensor for cyanide anion based on the PET effect in aqueous medium, *Sens. Actuators, B*, 2017, **241**, 430–437.

42 T. D. Ashton, K. A. Jolliffe and F. M. Pfeffer, Luminescent probes for the bioimaging of small anionic species in vitro and in vivo, *Chem. Soc. Rev.*, 2015, **44**, 4547–4595.

43 A. Liu, R. Ji and S. L. Shen, A ratiometric fluorescent probe for sensing sulfite based on pyrido [1,2–a] benzimidazole fluorophore, *New J. Chem.*, 2017, **41**, 10096–10100.

44 Y. Ge, P. Wei and T. Wang, A simple fluorescent probe for monitoring pH in cells based on new fluorophorepyrido [1,2–a] benzimidazole, *Sens. Actuators, B*, 2018, **254**, 314–320.

45 X. Chen, L. Wang, X. Yang and L. Tang, A new aggregation–induced emission active fluorescent probe for sensitive detection of cyanide, *Sens. Actuators, B*, 2017, **241**, 1043–1049.

46 W. C. Lin and J. W. Hu, A ratiometric chemodosimeter for highly selective naked–eye and fluorogenic detection of cyanide, *Anal. Chim. Acta*, 2015, **893**, 91–100.

47 R. Manivannan and Y. A. Son, Blue light emitting fluorophore for the effective detection of cyanide ion and electronic test kit development for real time measurement, *Dyes Pigm.*, 2023, **210**, 110941.

48 D. Jothi, S. Munusamy, S. Enbanathan and S. K. Iyer, A benzothiazole-based new fluorogenic chemosensor for the detection of CN^- and its real-time application in environmental water samples and living cells, *RSC Adv.*, 2022, **12**, 8570–8577.

49 S. D. Padghan, L. C. Wang, W. C. Lin, J. W. Hu, W. C. Liu and K. Y. Chen, Rational design of an ICT-based chemodosimeter with aggregation-induced emission for colorimetric and ratiometric fluorescent detection of cyanide in a wide pH range, *ACS Omega*, 2021, **6**, 5287–5296.

50 S. D. Padghan, C. Y. Wang, W. C. Liu, S. S. Sun, K. M. Liu and K. Y. Chen, A naphthalene-based colorimetric and fluorometric dual-channel chemodosimeter for sensing cyanide in a wide pH range, *Dyes Pigm.*, 2020, **183**, 108724.

51 D. Tamilarasan, R. Suhasini, V. Thiagarajan and R. Balamurugan, Reversible Addition of Cyanide to Triphenylamine Attached Difluoroboron β-Diketonate Facilitated Selective Colorimetric and Fluorimetric Detection of Cyanide Ion, *Eur. J. Org. Chem.*, 2020, **2020**, 993–1000.

52 L. Hou, F. Li, J. Guo, X. Zhang, X. Kong, X. T. Cui, C. Dong, Y. Wang and S. Shuang, A colorimetric and ratiometric fluorescent probe for cyanide sensing in aqueous media and live cells, *J. Mater. Chem. B*, 2019, **7**, 4620–4629.

53 A. Ozdemir and S. Erdemir, Phenanthroimidazole and dicyanovinyl-substituted triphenylamine for the selective detection of CN^-; DFT calculations and practically applications, *J. Photochem. Photobiol., A*, 2020, **390**, 112328.

54 A. Tigreros, J. C. Castillo and J. Portilla, Cyanide chemosensors based on 3-dicyanovinylpyrazolo[1,5-a] pyrimidines: Effects of peripheral 4-anisyl group substitution on the photophysical properties, *Talanta*, 2020, **215**, 120905.

55 T. S. Reddy and M. S. Choi, Dicyanovinylcoumarin as a turn-on fluorescent sensor for cyanide ion, *J. Photochem. Photobiol., A*, 2018, **351**, 108–114.

56 Y. Zhang, D. Yu and G. Feng, Colorimetric and near infrared fluorescent detection of cyanide by a new phenanthro imidazole–indolium conjugated probe, *RSC Adv.*, 2014, **4**, 14752–14757.

© 2024 The Author(s). Published by the Royal Society of Chemistry

Open Access Article. Published on 23 May 2024. Downloaded on 2/10/2026 11:50:29 PM. This article is licensed under a Creative Commons Attribution 3.0 Unported Licence.

57 Y. Shiraishi, M. Nakamura, K. Yamamoto and T. Hirai, Rapid selective, and sensitive fluorometric detection of cyanide anions in aqueous media by cyanine dyes with indolium–coumarin linkages, *Chem. Commun.*, 2014, **78**, 11583–11586.

58 A. Dvivedi, P. Rajakannu and M. Ravikanth, Meso-salicylaldehyde substituted BODIPY as a chemodosimetric sensor for cyanide anions, *Dalton Trans.*, 2015, **44**, 4054–4062.

59 M. K. Bera, C. Chakraborty, P. K. Singh, C. Sahu, K. Sen, S. Maji, A. K. Das and S. Malik, Fluorene-based chemodosimeter for "turn-on" sensing of cyanide by hampering ESIPT and live cell imaging, *J. Mater. Chem. B*, 2014, **2**, 4733–4739.

60 S. Pramanik, V. Bhalla and M. Kumar, Hexaphenyl benzene-based fluorescent aggregates for ratio-metric detection of cyanide ions at nanomolar level: set–reset memorized sequential logic device, *ACS Appl. Mater. Interfaces*, 2014, **6**, 5930–5939.

61 Y. Sun, G. Wang and W. Guo, Colorimetric detection of cyanide with N-nitrophenyl benzamide derivatives, *Tetrahedron Lett.*, 2009, **65**, 3480–3485.

62 Y. Kim, H. Zhao and F. P. Gabbaï, Sulfonium boranes for the selective capture of cyanide ions in water, *Angew. Chem., Int. Ed.*, 2009, **48**, 4957–4960.

63 Z. Yu, Z. Zheng, M. Yang, L. Wang, Y. Tian, J. Wu, H. Zhou, H. Xu and Z. Wu, Photon-induced intramolecular charge transfer with the influence of D/A group and mode: optical physical properties and bio-imaging, *J. Mater. Chem. C*, 2013, **1**, 7026–7033.

64 A. Biswas, A. Maji, S. Gharami and T. K. Mondal, An ICT-based organic framework for the fluorogenic detection of lethal pulmonary agent phosgene, *New J. Chem.*, 2023, **47**, 14154.

65 R. Quevedo, ^{1}H- and ^{13}C-NMR spectroscopic study of intermolecular interactions between tyrosine-derived azacyclophanes and aromatic rings, *J. Mol. Struct.*, 2020, **1207**, 127777.

66 S. Cheng, A. Li, X. Pan, H. Wang, C. Zhang, J. Li and X. Qi, A near-infrared fluorescent probe for highly specific and ultrasensitive detection of hypochlorite ions in living cells, *Anal. Bioanal. Chem.*, 2021, **413**, 4441–4450.

67 X. Pan, S. Cheng, C. Zhang and X. Qi, Two highly sensitive fluorescent probes based on cinnamaldehyde with large Stokes shift for sensing of HSO_3^- in pure water and living cells, *Anal. Bioanal. Chem.*, 2020, **412**, 6959–6968.

68 R. Bhaskar and S. Sarveswari, Colorimetric sensor for real-time detection of cyanide ion in water and food samples, *Inorg. Chem. Commun.*, 2019, **102**, 83–89.

69 X. Wu, J. Chen and J. X. Zhao, A reversible fluorescent logic gate for sensing mercury and iodide ions based on a molecular beacon, *Analyst*, 2013, **138**, 5281–5287.

70 S. Qu, C. Zheng, G. Liao, C. Fan, G. Liu and S. Pu, A fluorescent chemosensor for Sn^{2+} and Cu^{2+} based on a carbazole-containing diarylethene, *RSC Adv.*, 2017, **7**, 9833–9839.

71 M. J. Frisch, G. W. Trucks, H. B. Schlegel, G. E. Scuseria, M. A. Robb, J. R. Cheeseman, G. Scalmani, V. Barone, B. Mennucci, G. A. Petersson, H. Nakatsuji, M. Caricato, X. Li, H. P. Hratchian, A. F. Izmaylov, J. Bloino, G. Zheng, J. L. Sonnenberg, M. Hada, M. Ehara, K. Toyota, R. Fukuda, J. Hasegawa, M. Ishida, T. Nakajima, Y. Honda, O. Kitao, H. Nakai, T. Vreven, J. A. Montgomery, Jr., J. E. Peralta, F. Ogliaro, M. Bearpark, J. J. Heyd, E. Brothers, K. N. Kudin, V. N. Staroverov, R. Kobayashi, J. Normand, K. Raghavachari, A. Rendell, J. C. Burant, S. S. Iyengar, J. Tomasi, M. Cossi, N. Rega, J. M. Millam, M. Klene, J. E. Knox, J. B. Cross, V. Bakken, C. Adamo, J. Jaramillo, R. Gomperts, R. E. Stratmann, O. Yazyev, A. J. Austin, R. Cammi, C. Pomelli, J. W. Ochterski, R. L. Martin, K. Morokuma, V. G. Zakrzewski, G. A. Voth, P. Salvador, J. J. Dannenberg, S. Dapprich, A. D. Daniels, Ö. Farkas, J. B. Foresman, J. V. Ortiz, J. Cioslowski and D. J. Fox, *Gaussian 09, Revision D.01*, Gaussian, Inc., Wallingford CT, 2009.

72 A. D. Becke, Density-functional thermochemistry. III. The role of exact exchange, *J. Chem. Phys.*, 1993, **98**, 5648–5652.

73 C. Lee, W. Yang and R. G. Parr, Development of the Colle-Salvetti correlation-energy formula into a functional of the electron density, *Phys. Rev. B: Condens. Matter Mater. Phys.*, 1988, **37**, 785–789.

74 F. Furche and R. Ahlrichs, Adiabatic time-dependent density functional methods for excited state properties, *J. Chem. Phys.*, 2002, **117**, 7433–7447.

75 R. Bauernschmitt and R. Ahlrichs, Treatment of electronic excitations within the adiabatic approximation of time dependent density functional theory, *Chem. Phys. Lett.*, 1996, **256**, 454–464.

76 R. E. Stratmann, G. E. Scuseria and M. J. Frisch, An efficient implementation of time-dependent density-functional theory for the calculation of excitation energies of large molecules, *J. Chem. Phys.*, 1998, **109**, 8218–8224.

77 M. E. Casida, C. Jamorski, K. C. Casida and D. R. Salahub, Molecular excitation energies to high-lying bound states from time-dependent density-functional response theory: Characterization and correction of the time-dependent local density approximation ionization threshold, *J. Chem. Phys.*, 1998, **108**, 4439–4449.

78 M. Cossi and V. Barone, Time-dependent density functional theory for molecules in liquid solutions, *J. Chem. Phys.*, 2001, **115**, 4708–4717.

79 V. Barone and M. Cossi, Quantum calculation of molecular energies and energy gradients in solution by a conductor solvent model, *J. Phys. Chem. A*, 1998, **102**, 1995–2001.

80 M. Cossi, N. Rega, G. Scalmani and V. Barone, Energies, structures, and electronic properties of molecules in solution with the C-PCM solvation model, *J. Comput. Chem.*, 2003, **24**, 669–681.

© 2024 The Author(s). Published by the Royal Society of Chemistry